International Journal of Industrial Chemistry (2019) 10:89–96
https://doi.org/10.1007/s40090-019-0174-7

RESEARCH

Combustion synthesis of porous MgO and its adsorption properties

Songnan Li[1]

Received: 27 March 2018 / Accepted: 18 February 2019 / Published online: 27 February 2019

Abstract

Porous magnesium oxide was synthesized by a combustion method, with $Mg(NO_3)_2$, ethylene glycol and deionized water as reactants, and characterized by X-ray diffraction, infrared spectroscopy, scanning electron microscopy, transmission electron microscopy and nitrogen sorption/desorption. The results showed that the as-prepared porous magnesium oxide has the multi-scale porous size with a large BET surface area of 203.8 $m^2\ g^{-1}$. Magnesium oxides synthesized with other reactants have rod-shaped and granular morphologies, and their BET surface areas are 17.6 and 3.4 $m^2\ g^{-1}$, respectively. Compared to the magnesium oxide with the low specific surface area, porous magnesium oxide exhibited higher adsorption efficiency with a maximum adsorption capacity of approximately 1088 mg g^{-1} in removing Congo red. The as-synthesized porous magnesium oxide could be used as an efficient adsorption material in Congo red removal from the wastewater.

Keywords MgO · Combustion synthesis · Porous material · Water treatment

Introduction

Textile, dyestuff manufacturing, paper industry, rubber and plastics industry will produce a large number of waste water containing dyes [1]. Except for visual reasons, the dyes can also be decomposed to produce various kinds of carcinogens, which is harmful to the environment and to the health of the human being [2, 3]. Therefore, dyes containing wastewater must be harmless disposal before discharge. At present, there are a variety of ways to deal with dyes wastewater, such as adsorption, photocatalytic degradation, activated sludge, coagulation, ozonation, electrochemical and ultrasonic techniques [4–7]. Among these methods for the treatment of the dyes, the adsorption method has received more attention due to its simplicity, efficiency and availability of variety of adsorbents. Among these readily available adsorbent materials, such as, layered double hydroxides, zeolites, metal oxides, metal oxides are more advantageous due to its cheap value and easy to synthesize [8–10]. The applications of the metal oxides synthesized by solution combustion method have been reviewed by Li et al. [11]. And, Li et al. studied the antibacterial properties of magnesium oxide with surface oxygen vacancies synthesized by this method [12]. Using this method, $BiOBr/Bi_{24}O_{31}Br_{10}$ heterojunctions with oxygen vacancies have also been synthesized in Li's report [13]. As a common oxide, magnesium oxide has been used in the different area such as catalytic and adsorption field. Porous magnesium oxides can provide more contact sites to improve the treatment effect [14, 15]. Different methods have been used to synthesize porous magnesium oxides [16, 17]. Klabunde et al. have done a lot of research on the synthesis and application of magnesium oxide. For example, they were investigated the effect of the crystallites of magnesium oxide on the catalytic performance and the effect of vanadium and carbon doping on the adsorption properties of magnesium oxide [18, 19]. Using SBA-15 and CMK-3 as hard template, mesoporous MgO was synthesized in Tiemann's report [20]. Flower-like size MgO sphere and its composites with hierarchical structure were synthesized using ethylene glycol as addition agent in Zhu's report [21]. And, the products exhibited excellent adsorption capacity for dye. Hu et al. reported a one-step method for preparation of the MgO–SiO_2 composites with rough surfaces. The adsorption kinetics of the composite for CR were studied in his report [22]. Porous MgO with a specific surface area of 72 m^2/g has been synthesized using a surfactant-assisted

Electronic supplementary material The online version of this article (https://doi.org/10.1007/s40090-019-0174-7) contains supplementary material, which is available to authorized users.

✉ Songnan Li
ok19841210@163.com

[1] Modern Experiment Center, Harbin Normal University, Harbin 150025, People's Republic of China

method following hydrothermal-treatment in Wang's report [23]. The as-prepared MgO exhibited good removal rate for Congo red. Avillez et al. used polyvinyl alcohol as a precursor to synthesise nanosize MgO with a special surface area of 82 m^2 g^{-1} by a combustion method [24]. Using different reagents as fuels, a hybrid sol–gel combustion method has been used to synthesise MgO with variable crystallite size in Nassar's report [25]. However, a little research has been done on the removal of dye contaminants by porous MgO synthesized by combustion method.

In this study, a facile combustion process was used to synthesise porous MgO using magnesium nitrate, glycerol and deionized water as raw materials, and used other raw materials in comparison test. The structure, morphology and surface properties of the as-prepared porous magnesium oxides were studied by a series of characterization, such as XRD, SEM and many more. Finally, the adsorption properties of the material on Congo red were studied in detail.

Experimental section

Materials

Magnesium nitrate, magnesium hydroxide and ethylene glycol were purchased from Sinopharm Chemical Reagent Co., Ltd., Shanghai, China. All chemicals were used directly without further purification.

Synthesis of porous magnesium oxide

Magnesium nitrate (1.28 g) was added to a 4 mL mixed solution containing ethylene glycol and deionized water with a volume ratio of 1:1. After stirring for 30 min, the solution (without drying) was transferred into the crucible and calcined at 600 °C for 2 h in a muffle furnace. The obtained white fluffy-like powder was marked as P-MgO and used for characterization and adsorption. In addition, magnesium nitrate and magnesium hydroxide are used as raw materials for comparison test. Raw materials (2.00 g) were put into the crucible and calcined at 600 °C for 2 h in a muffle furnace. The obtained white powder was marked as N-MgO and H-MgO.

Characterizations

X-ray diffraction measurements are carried out on a Bruker D8 advance diffractometer, Fourier-transform infrared (FTIR) spectra are collected on a VERTEX80 spectrophotometer using KBr pellets. The morphology was characterized by transmission electron microscopy (TEM, Hitachi H-7650, 100 kV) and scanning electron microscopy (SEM, Hitachi S-4800 microscope). The Brunauer–Emmett–Teller (BET) specific surface areas of the products are analyzed by nitrogen adsorption in a NOVA 2000 nitrogen adsorption apparatus. The concentration of the Congo red dyes are analyzed with a Agilent Cary4000 spectrophotometer, measuring the absorbance at k_{max} = 488 nm, using the appropriate calibration curve.

Removal of Congo red

The removal studies were carried out in a series of 100 mL Cone bottle by giving a suitable shaking time with a given dose of adsorbent together with 100 mL Congo red solution. Batch equilibrium isotherms with different concentrations of Congo red were studied by contacting P-MgO (0.05 g) for 2 h at room temperature. After equilibration, the used P-MgO was separated from the solution by centrifugal, and the supernatant was analyzed by Cary4000 spectrophotometer. The amount of the Congo red loading (mg) per unit mass of P-MgO were obtained by formula (1) and (2), respectively. The formula has been listed in the supporting information.

Results and discussion

Powder X-ray diffraction

The XRD patterns of the as-prepared porous magnesium oxide (P-MgO, N-MgO, H-MgO) and P-MgO after adsorption of Congo red are shown in Fig. 1. All the peaks in diffraction patterns of P-MgO, N-MgO, H-MgO can be indexed to cubic magnesium oxide (JCPDS 45-0946) peaks, no other phases. The lattice parameters of as-prepared MgO were

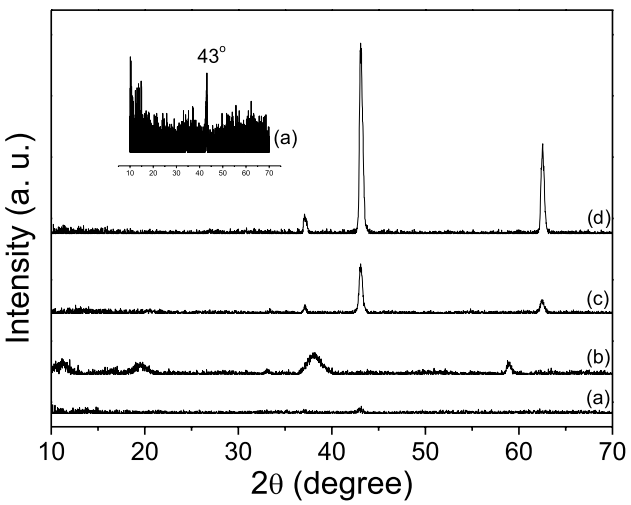

Fig. 1 Power XRD pattern of as-prepared porous magnesium oxide. **a** P-MgO, **c** N-MgO, **d** H-MgO and **b** P-MgO after adsorption of Congo red

close to the standard value (4.2212 Å) of the MgO phase (Table S1). This means that all the as-prepared magnesium oxide samples corresponded to pure MgO product. The possible combustion reaction is shown by the following equation:

$$Mg^{2+} + 2NO_3^- + O_2 + \left(CH_2OH\right)_2 \rightarrow MgO \downarrow + H_2O \uparrow + CO_2 \uparrow + NO_x \uparrow . \quad (1)$$

The crystallinity of the P-MgO is lower to the others, which may be caused by the gas produced during the combustion process inhibits the crystal growth. This defective crystal may be more advantageous for adsorption due to its higher surface energy. After adsorption of Congo red at the condition of P-MgO 0.1 g, 100 mL, $C_0 = 2000$ mg/L, adsorption time 24 h, pH = 7, the XRD pattern of the product is shown in Fig. 1b. It can be seen that the product is mainly magnesium hydroxide, which is the result of the reaction of magnesium oxide and water [26].

SEM and TEM

The SEM images of P-MgO show sponge-like morphology, which compose of nano-crystallites and different sizes of holes, seen in Fig. 2a. The TEM images can prove this result. Figure 3a, b shows that the P-MgO exhibits variety of nano-size bubble-like holes overlap each other, and the size of inner holes are larger than the lateral ones [27, 28]. This means that the crystal growth of P-MgO is not complete and the grain size is small, which agree well with the XRD result. The H-MgO has a morphology of a micrometer-sized aggregates consisting of irregular rod and piece. The size of rod is about 200 nm long and 50 nm wide and the piece is in micron-sized. The N-MgO has a morphology of irregular particles with a size of about 1 µm. The presence of ethylene glycol plays a key role, which gas combustion is the main factor of forming such a porous morphology.

Nitrogen adsorption–desorption

Nitrogen adsorption–desorption isotherms were used for testing the surface and the porous characteristics of the as-prepared porous magnesium oxide (P-MgO, N-MgO, H-MgO) and P-MgO after adsorption of Congo red as shown in Figs. 4 and 5. All of the samples show type IV isotherm curve due to the obvious hysteresis loops, the inset figure shows the hysteresis loops of the samples of N-MgO and H-MgO [29]. However, the as-prepared porous magnesium oxides have different types of hysteresis loops. P-MgO has a H2(b)-type hysteresis loop which means the material has an ink bottle like porous with wide bottleneck. N-MgO and H-MgO have H3-type hysteresis loop. H3-type hysteresis loop indicates that the material has a structure of piece agglomeration. P-MgO after adsorption of Congo red has a H3-type hysteresis loop [30].

The BET surface areas of as-prepared porous magnesium oxide (P-MgO, H-MgO, N-MgO) and P-MgO after adsorption of Congo red are 203.8, 17.6, 3.4 and 111 m^2/g, respectively (listed in Table 1). The pore diameters of as-prepared porous magnesium oxide are found to be around 3–4 nm. The pore diameters curve of P-MgO has a major peak at 4 nm and distributed in the range of 1–3 nm, in the range of 20–50 nm also have a certain distribution. After adsorption of Congo red, the distribution of pores in the range of 1–3 nm disappeared and replaced by a new distribution in the range of 4–15 nm with a peak at 7 nm. The distribution of other pore sizes has not changed. This indicates that the pore structure of P-MgO undergoes a change during the adsorption process, the micro-pores are filled with the adsorbate, and during the formation of magnesium hydroxide process, some mesopores formed by the stacking of the sheet-like products.

FT-IR

The FT-IR spectra of the as-prepared porous magnesium oxide (P-MgO, N-MgO, H-MgO) and P-MgO after adsorption of Congo red are shown in Fig. 6. The strong adsorption bands peak central at 3450 m^{-1} for all the samples are corresponding to the stretching mode of –OH stretching mode of the hydroxyl groups present on the surface due to the chemical adsorption of water on the surface [31]. The surface of MgO has acid–base properties, which makes it the ability to adsorb carbon dioxide in the air. The peak at 1451 cm^{-1} corresponding to the asymmetric stretching vibration of adsorbed carbon dioxide [32]. The bands in between 900 and 400 cm^{-1} are due to characteristic stretching of the Mg–O bond in MgO structure. After adsorption of Congo red, the new adsorption bands at 1056, 1124, and 1236 cm^{-1} are attributed to stretching vibration of sulfur–oxygen double bond. The adsorption bands at 3660 and 1640 are attributed to O–H stretching vibration of $Mg(OH)_2$ produced by reacting P-MgO with water [33].

Effect of initial pH

The pH is an important factor affecting the adsorption of Congo red on the adsorbents [34]. Experiments were carried out using a constant temperature water bath oscillator and 0.05 g of P-MgO at room temperature to study the initial pH effect in the adsorption process. A volume of 50 mL of Congo red at a concentration of 500 mg L^{-1} was used, with a stirring at different pH for 6 h. The effect of pH on removal of Congo red on P-MgO is shown in Fig. S1. It can be seen that the pH has a little influence on

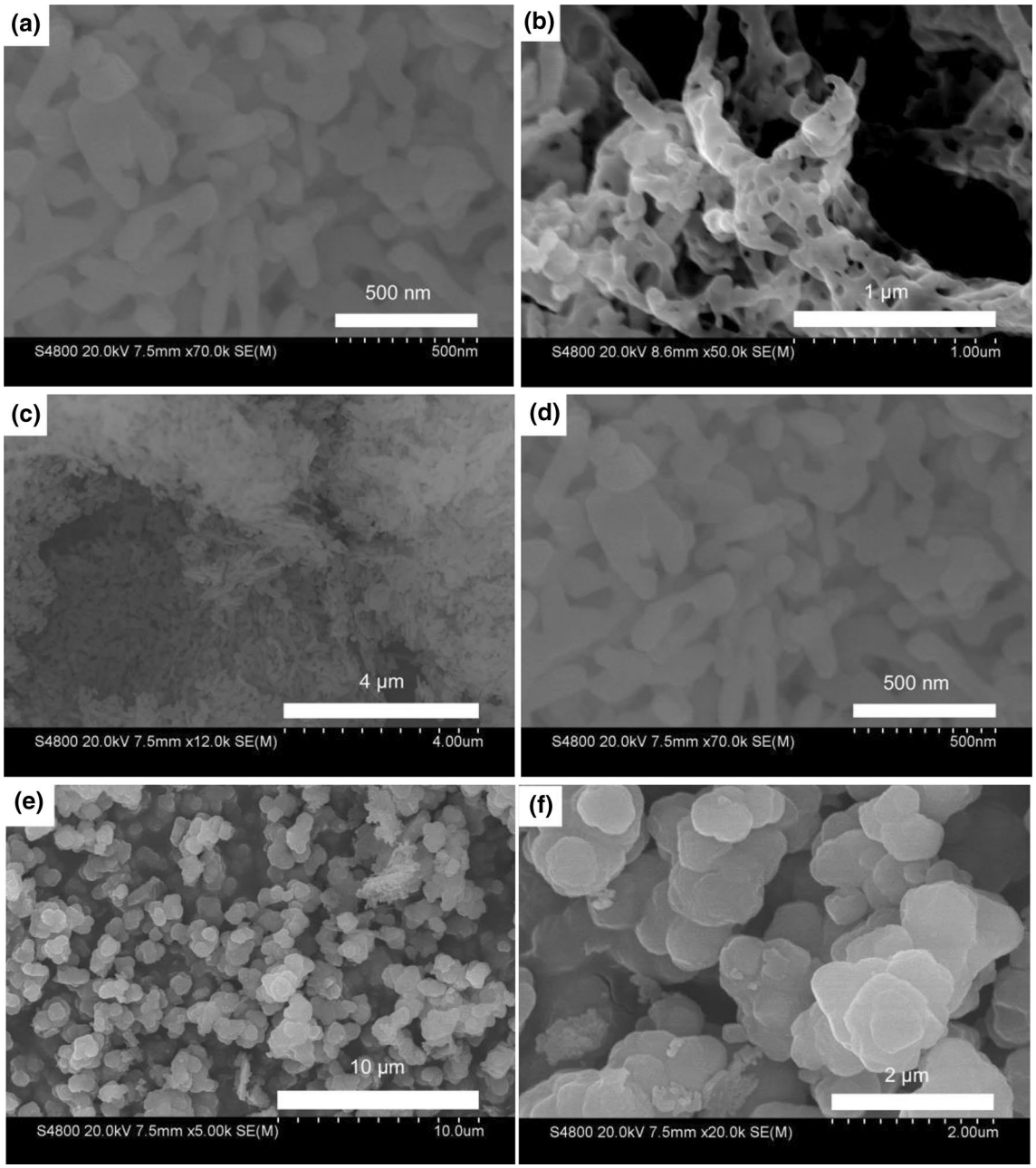

Fig. 2 SEM images of as-prepared porous magnesium oxide. **a**, **b** P-MgO, **c**, **d** N-MgO, **e**, **f** H-MgO

the removal rate and adsorption capacity. It is due to the magnesium hydroxide formed during the reaction process has a moderating effect on pH, which allows the pH of the solution to react within a certain range. This process reduces the effect of solution pH on adsorption.

Effect of adsorbent dose

The effect of P-MgO dose on the removal rate and adsorption capacity was studied at different dose (0.01–0.1 g) and is presented in Fig. S2. A volume of 100 mL of Congo red

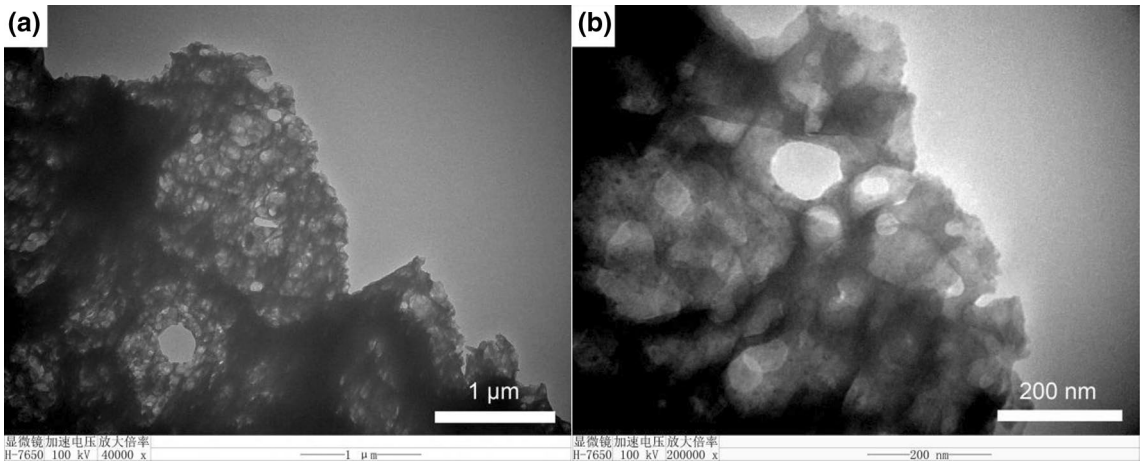

Fig. 3 TEM images of as-prepared P-MgO

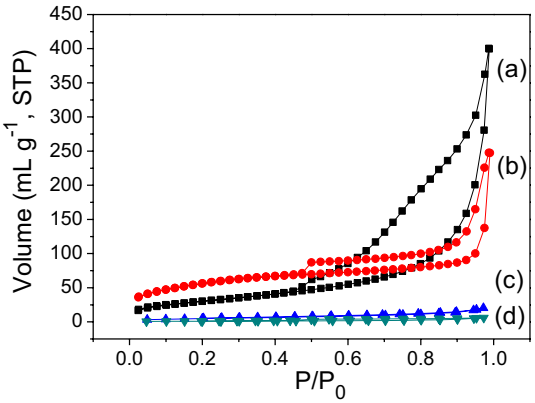

Fig. 4 N_2 adsorption–desorption isotherms of as-prepared porous magnesium oxide. **a** P-MgO, **c** N-MgO, **d** H-MgO and **b** P-MgO after adsorption of Congo red

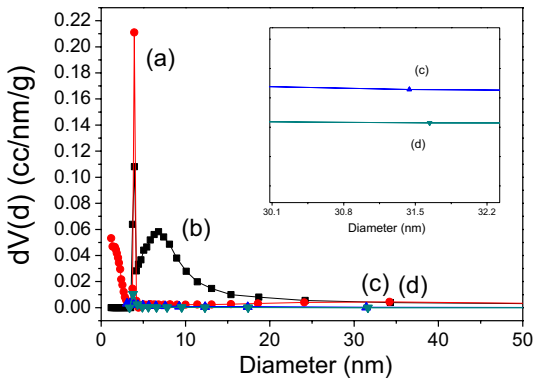

Fig. 5 Pore-size distributions of as-prepared porous magnesium oxide. **a** P-MgO, **c** N-MgO, **d** H-MgO and **b** P-MgO after adsorption of Congo red

Table 1 BET surface areas and pore parameters of different samples

Sample	P-MgO	H-MgO	N-MgO	P-MgO after removal of CR
S_{BET} (m^2/g)[a]	203.8	17.6	3.4	111.3
V_P (cm^3/g)[b]	0.389	0.027	0.010	0.696
d_P (nm)[b]	3.9	3.1	3.8	3.9

[a]Performed by multipoint BET method

[b]Cumulative desorption pore volume and average pore diameter performed by BJH method

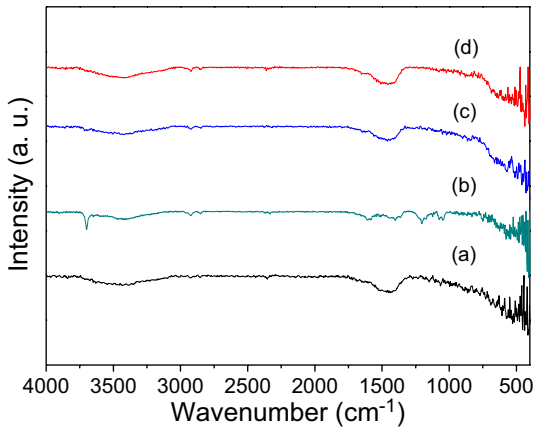

Fig. 6 FT-IR patterns of as-prepared P-MgO. **a** P-MgO, **c** N-MgO, **d** H-MgO and **b** P-MgO after adsorption of Congo red

at a concentration of 500 mg L^{-1} was used, with a stirring for 6 h. The result shows that the removal rate increased from 10 to 99% when the amount of adsorbent increased from 0.01 to 0.1 g, due to an increase in the number of available adsorption sites [35]. However, the adsorption

Table 2 Isotherm parameters for adsorption of Congo red on P-MgO

	Freundlich			Langmuir		
	k_F	n	R^2	q_{max} (mg/g)	b (L/mg)	R^2
25	116	0.45	0.64	1032	0.078	0.997
35	133	0.44	0.63	1055	0.098	0.998
45	159	0.41	0.55	1088	0.114	0.997

Table 3 Thermodynamic parameters for adsorption of Congo red on P-MgO

Temp (°C)	ΔG^0 (kJ/mol)	ΔH^0 (kJ/mol)	ΔS^0 (J/mol/K)
25	−1.71	7.45	30.76
35	−2.02		
45	−2.33		

capacity exhibits an opposite behavior to the removal percent, which may be due to an increase in the mass of the adsorbent at a defined dye concentration.

Effect of initial concentration

The effect of initial concentration of Congo red on adsorption was investigated in the concentration range from 50 to 1500 mg L^{-1} for 6 h at different temperature (Fig. S3). Adsorption capacity increases with the initial concentration of Congo red, and after a certain equilibrium concentration, the adsorption capacity becomes constant [36].

Adsorption isotherms

Based on the above adsorption data, the Langmuir and the Freundlich isotherm equations were used to simulate the isotherms, equations are shown in Supporting Information. All the isotherm parameters calculated from the two isotherm equations are listed in Table 2. By comparing the linear regression coefficients, we can see that the result of the Langmuir isotherm equation is much higher than those of the Freundlich model, which suggested that the adsorption process of Congo red on P-MgO is monolayer adsorption. To imitate the adsorption process of Congo red on P-MgO, the thermodynamic parameters (ΔG^0, ΔH^0 and ΔS^0) were calculated from thermodynamics equations (seen in Supporting Information) and listed in Table, Figures seen in Fig. S4–6. According to the results from calculation (seen in Table 3), the negative Gibbs free energy, positive enthalpy and positive entropy can explain that the adsorption process is a spontaneous, endothermic process, and the adsorption reaction more favorable at higher temperature [37].

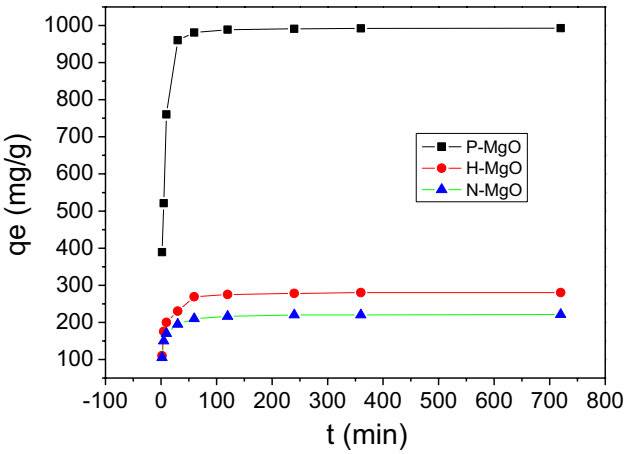

Fig. 7 Effect of reaction time on the adsorption of Congo red by P-MgO, H-MgO, N-MgO. Adsorption dosage 0.05 g, C_0 = 1200 mg/L, adsorption time 10 min–24 h, pH = 7

Effect of contact time

Figure S7 shows the effect of the time on the adsorption of Congo red onto P-MgO at different temperature, the initial concentration of Congo red is 1200 mg L^{-1}. Like the vast majority of the adsorption process, the adsorption capacity of Congo red onto P-MgO increases with increasing adsorption time, and reaches the equilibrium at 60 min [38].

As a comparative test, the same experimental conditions were used to test the adsorption properties of the other two adsorbents, seen in Fig. 7. Under the same conditions, the equilibrium adsorption capacities of the two materials for Congo red were 190 and 210 mg g^{-1}, respectively. This result is much smaller than that of P-MgO. As discussed above, the P-MgO has a porous structure with larger BET surface area than that of N-MgO and H-MgO, giving it a higher adsorption ability.

Adsorption kinetics

The pseudo-first-order and pseudo-second-order kinetics equations are used to identify the kinetics of the adsorption process, equations are shown in Supporting Information,

Table 4 Kinetic parameters for adsorption of Congo red on P-MgO

Parameters		Co	
Temp (°C)	25	35	45
Pseudo-first-order			
k_1 (min^{-1})	0.0076	0.0085	0.0090
R^2	0.48	0.56	0.61
q_e (cal) (mg g^{-1})	308	326	367
Pseudo-second-order			
k_2 (g mg^{-1} min^{-1})	0.00015	0.00014	0.00012
R^2	0.9995	0.9996	0.9997
q_e (cal) (mg g^{-1})	1007	1039	1074

seen in Fig. S8–9. The calculated kinetic model constants (Table 4) indicate that the experimental data fit better with the pseudo-second-order kinetic model with regression coefficients are 0.9995, 0.9996, 0.9997, respectively. This result means that the adsorption process is boundary layer and surface adsorption chemisorption [39].

Regeneration

After regeneration by calcination at 600 °C for 1 h, the recycled P-MgO is used for studying the removal rate in a number of regeneration cycles. As shown in Fig. S10, the removal rate of P-MgO in the first cycle is 78.9% in CR solution with an initial concentration of 2000 mg L^{-1}, indicating that the damaged material structure is not conducive to adsorption, which leads to a reduction in the removal rate.

Conclusion

In conclusion, porous magnesium oxide was successful synthesized and well characterized. The present study shows that the porous magnesium oxide has a good adsorption capacity for Congo red. The adsorption kinetic of Congo red is in good agreement with pseudo-second-order kinetic model, and adsorption behavior can be well described by the Langmuir adsorption model. The results show that the adsorption process is spontaneous and exothermic, and a maximum adsorption capacity of 1088 mg g^{-1} was calculated from the above model.

Acknowledgements This work was supported by National Natural Science Foundation of China (21671050), National Natural Science Foundation of China (21771047).

References

1. Raval NP, Shah PU, Shah NK (2016) Adsorptive amputation of hazardous azo dye Congo red from wastewater: a critical review. Environ Sci Pollut Res 23:14810–14853
2. Mahapatra A, Mishra BG, Hota G (2013) Adsorptive removal of Congo red dye from wastewater by mixed iron oxide–alumina nanocomposites. Ceram Int 39:5443–5451
3. Abdelkader E, Nadjia L, Rose-Noëlle V (2016) Adsorption of Congo red azo dye on nanosized SnO_2 derived from sol–gel method. Int J Ind Chem 7:53
4. Ahmed MA, Abou-Gamra ZM (2016) Mesoporous MgO nanoparticles as a potential sorbent for removal of fast orange and bromophenol blue dyes. Nanotechnol Environ Eng 1:10
5. Mageshwari K, Mali SS, Sathyamoorthy R, Patil PS (2013) Template-free synthesis of MgO nanoparticles for effective photocatalytic applications. Powder Technol 249:456–462
6. Qu X, Alvarez JJ, Li Q (2013) Applications of nanotechnology in water and wastewater treatment. Water Res 47:3931–3946
7. Fajardo AS, Rui CM, Silva DR, Martínez-Huitle CA, Quinta-Ferreira RM (2017) Dye wastewaters treatment using batch and recirculation flow electrocoagulat. J Electroanal Chem 801:30–37
8. Wawrzkiewicz M, Wiśniewska M, Wołowicz A, Gun'Ko VM, Zarko VI (2017) Mixed silica-alumina oxide as sorbent for dyes and metal ions removal from aqueous solutions and wastewaters. Microporous Mesoporous Mater 250:128–147
9. Huang W, Yu X, Li D (2015) Adsorption removal of Congo red over flower-like porous microspheres derived from Ni/Al layered double hydroxide. RSC Adv 5:84937
10. Shah BA, Patel HD, Shah AV (2011) Equilibrium and kinetic studies of the adsorption of basic dye from aqueous solutions by zeolite synthesized from bagasse fly ash. Environ Prog Sustain 30:549–557
11. Li FT, Ran JR, Jaroniec M, Qiao SZ (2015) Solution combustion synthesis of metal oxide nanomaterials for energy storage and conversion. Nanoscale 7:17590–17610
12. Hao YJ, Liu B, Tian LG, Li FT, Ren J, Liu SJ, Liu Y, Zhao J, Wang XJ (2017) Synthesis of 111 facet-exposed MgO with surface oxygen vacancies for ROS generation in the dark. ACS Appl Mater Interfaces 9(14):12687–12693
13. Li FT, Wang Q, Ran JR, Hao YJ, Wang XJ, Zhao DS, Qiao SZ (2015) Ionic liquids self-combustion synthesis of BiOBr/$Bi_{24}O_{31}Br$ 10 heterojunctions with exceptional visible-light photocatalytic performances. Nanoscale 7:1116–1126
14. Pilarska AA, Klapiszewski Ł, Jesionowski T (2017) Recent developments in the synthesis, modification and application of $Mg(OH)_2$ and MgO: a review. Powder Technol 319:373–407
15. Najafi A (2017) A novel synthesis method of hierarchical mesoporous MgO nanoflakes employing carbon nanoparticles as the hard templates for photocatalytic degradation. Ceram Int 43:5813–5818
16. Lv Z, Wang H, Chen C, Yang S, Chen L, Alsaedie A, Hayat T (2019) Enhanced removal of uranium(VI) from aqueous solution

by a novel Mg-MOF-74-derived porous MgO/carbon adsorbent. J Colloid Interface Sci 537:A1–A10
17. Chowdhury AH, Chowdhury IH, Naskar MK (2014) A facile synthesis of grainy rod-like porous MgO. Mater Lett 158:190–193
18. Choudary BM, Mulukutla RS, Klabunde KJ (2003) Benzylation of aromatic compounds with different crystallites of MgO. J Am Chem Soc 125:2020–2021
19. Bedilo AF, Shuvarakova EI, Volodin AM, Ilyina EV, Mishakov IV, Vedyagin AA, Chesnokov VV, Heroux DS, Klabunde KJ (2014) Effect of modification with vanadium or carbon on destructive sorption of halocarbons over nanocrystalline MgO: the role of active sites in initiation of the solid-state reaction. J Phys Chem C 118:13715–13725
20. Roggenbuck J, Tiemann M (2005) Ordered mesoporous magnesium oxide with high thermal stability synthesized by exotemplating using CMK-3 carbon. J Am Chem Soc 127:1096–1097
21. Xu J, Xu DF, Zhu BC, Cheng B, Jiang CJ (2018) Adsorptive removal of an anionic dye Congo red by flower-like hierarchical magnesium oxide (MgO)–graphene oxide composite microspheres. Appl Surf Sci 435:1136–1142
22. Hu MQ, Yan XL, Hu XY, Zhang JJ, Feng R, Zhou M (2018) Ultrahigh adsorption capacity of MgO/SiO_2 composites with rough surfaces for Congo red removal from water. J Colloid Interf Sci 510:111–117
23. Wang S, Li G, Xu W, Liu C, Dai L, Zhu H (2016) Facile preparation and application of magnesium hydroxide assembly spheres. Res Chem Intermed 42:2661–2668
24. Bueno AR, Oman FM, Jardim PM, Rey NA, Avillez RR (2014) Kinetics of nanocrystalline MgO growth by the sol–gel combustion method. Microporous Mesoporous Mater 185:86–91
25. Nassar MY, Mohamed TY, Ahmed IS, Samir I (2017) MgO nanostructure via a sol–gel combustion synthesis method using different fuels: an efficient nano-adsorbent for the removal of some anionic textile Dyes. J Mol Liq 225:730–740
26. El-Nahas S, Abdelkader A, Halawy SA, Mohamed MA (2017) Nanocrystalline MgO samples (115 and 126 nm) derived from two different precursors: characterization and catalytic activity. J Therm Anal Calorim 129:1313–1322
27. Liu Q, Yu J, Zhang X, Wang J, Li Z, Zhou J, Liu J, Gao Z, Yang W, Han S (2013) Hierarchically porous MgAl mixed metal oxide synthesized by sudden decomposition of MgAl layered double hydroxide gel. New J Chem 37:2128–2132
28. Zhang L, Zhu W, Zhang H, Bi S, Zhang Q (2014) Hydrothermal–thermal conversion synthesis of hierarchical porous MgO microrods as efficient adsorbents for lead(II) and chromium(VI) removal. RSC Adv 4:30542–30550
29. Dhal JP, Sethi M, Mishra BG, Hota G (2015) MgO nanomaterials with different morphologies and their sorption capacity for removal of toxic dyes. Mater Lett 141:267–271
30. Shahid A, Lopez-Orozco S, Marthala VR, Hartmann M, Schwieger W (2017) Direct oxidation of benzene to phenol over hierarchical ZSM-5 zeolites prepared by sequential post synthesis modification. Microporous Mesoporous Mater 237:151–159
31. Lia M, Zhou N, Luo X, Zhang G, Xie Z, Xua L, Liu P (2016) Macroporous MgO monoliths prepared by sol–gel process with phase separation. Ceram Int 42:16368–16373
32. Feng J, Zou L, Wang Y, Li B, He X, Fan Z, Ren Y, Lv Y, Zhang M, Chen D (2015) Synthesis of high surface area, mesoporous MgO nanosheets with excellent adsorption capability for Ni(II) via a distillation treating. J Colloid Interface Sci 438:259–267
33. Lafi R, Charradi K, Djebbi MA, Amara ABH, Hafiane A (2016) Adsorption study of Congo red dye from aqueous solution to Mg–Al-layered double hydroxide. Adv Powder Technol 27:232–237
34. Tian P, Han X, Ning G, Fang H, Ye J, Gong W, Lin Y (2013) Synthesis of porous hierarchical MgO and its superb adsorption properties. ACS Appl Mater Interfaces 5:12411–12418
35. Wang X, Zhang Y, Hao C, Dai X, Zhou Z, Si N (2014) Ultrasonic-assisted synthesis of aminated lignin by a Mannich reaction and its decolorizing properties for anionic azo-dye. RSC Adv 4:28156–28164
36. Wang L, Yan Z, Qiao S, Lu GQ, Huang Y (2007) Structural and morphological transformations of mesostructured titanium phosphate through hydrothermal treatment. J Colloid Interface Sci 316:954–961
37. Mahmoud HR, Ibrahim SM, El-Molla SA (2016) Textile dye removal from aqueous solutions using cheap MgO nanomaterials: adsorption kinetics, isotherm studies and thermodynamics. Adv Powder Technol 27:223–231
38. Khitous M, Salem Z, Halliche D (2016) Removal of phosphate from industrial wastewater using uncalcined $MgAl–NO_3$ layered double hydroxide: batch study and modeling. Desalin Water Treat 57:15920–15931
39. González MA, Pavlovic I, Barriga C (2015) Cu (II), Pb(II) and Cd (II) sorption on different layered double hydroxides a kinetic and thermodynamic study and competing factors. Chem Eng J 269:221–228